

1

[ATLAS Semivisible Jets]

2

[Elena Laura Busch]

3

Submitted in partial fulfillment of the
requirements for the degree of
Doctor of Philosophy
under the Executive Committee
of the Graduate School of Arts and Sciences

4

5

6

7

8

COLUMBIA UNIVERSITY

9

2024

10

© 2024

11

[Elena Laura Busch]

12

All Rights Reserved

13

Abstract

14

[ATLAS Semivisible Jets]

15

[Elena Laura Busch]

16

Abstract of dissertation (place-holder).

Table of Contents

18	Acknowledgments	v
19	Dedication	vi
20	Introduction or Preface	1
21	Chapter 1: The Standard Model	2
22	Chapter 2: The Large Hadron Collider	4
23	2.1 LHC Timeline	4
24	2.2 Accelerator Physics	5
25	2.2.1 The Journey of a Proton	5
26	2.2.2 Magnets	7
27	2.3 Luminosity	8
28	Chapter 3: The ATLAS Detector	10
29	3.1 Coordinate System and Geometry	10
30	3.2 Inner Detector	12
31	3.2.1 Pixel Detector	12
32	3.2.2 Semiconductor Tracker	13
33	3.2.3 Transition Radiation Tracker	13

34	3.3 Calorimeters	14
35	3.3.1 Liquid Argon Calorimeter	15
36	3.3.2 Tile Calorimeter	18
37	3.4 Muon Spectrometer	19
38	3.5 Magnet System	21
39	3.6 Forward Detectors	22
40	3.7 Trigger and Data Acquisition	23
41	Conclusion or Epilogue	26
42	References	30
43	Appendix A: Experimental Equipment	32
44	Appendix B: Data Processing	33

List of Figures

46	2.1	Timeline of LHC activities [9]	5
47	2.2	The LHC accelerator complex at CERN [11]	6
48	2.3	The octants of the LHC and location of various beam activities [10]	8
49	3.1	ATLAS coordinate system and geometry	12
50	3.2	A 3D visualization of the structure of the ID in the barrel region [13]	13
51	3.3	ATLAS calorimetery system [14]	14
52	3.4	Diagram of a segment of the EMB, demonstrating the accordion plate arrangement [15]	16
54	3.5	A LAr pulse as produced in the detector (triangle) and after shaping (curve) [15]	17
55	3.6	Readout gap structure in HEC [15]	17
56	3.7	TileCal wedge module [18]	19
57	3.8	Cross section view of the muon spectrometer system [19]	20
58	3.9	Layout of the barrel and endcap toroid magnets [22]	22

List of Tables

60

Acknowledgements

61 Insert your acknowledgements text here. This page is optional, you may delete it if not
62 needed.

63

Dedication

64

Dedicated to my friends and family

65

Introduction or Preface

66 Insert your preface text here if applicable. This page is optional, you may delete it if not
67 needed. If you delete this page make sure to move page counter comment in thesis.tex to correct
68 location.

69

70

Chapter 1: The Standard Model

71 Four fundamental forces

72 The Standard Model is a universally accepted framework which explains most of the interactions of fundamental particles. The SM is a renormalizable quantum field theory that obeys the local symmetry G_{SM} :

$$G_{SM} = SU(3)_C \times SU(2)_L \times U(1)_Y \quad (1.1)$$

75 The $SU(3)_C$ symmetry component is the non-Abelian gauge group of quantum chromodynamics (QCD), the theory of strong interactions. There are 8 generators for the $SU_C(3)$ group which 76 correspond to *gluons*, massless spin-1 gauge boson which carry the force of the strong interaction.

77 Gluon and quarks, the particles which interact with the strong force, carry a color charge C .

79 The $SU(2)_L \times U(1)_Y$ symmetry group represents the electroweak sector of the Standard Model. 80 There are 4 generators for this group, which correspond to the four massless gauge bosons W^1 , W^2 , 81 W^3 , and B. From these massless gauge bosons are formed the massive mediators of the weak force, 82 the W^- , W^+ and Z^0 bosons, and the massless electromagnetic force carrier, the photon γ .

83 The interplay between the fermionic and bosonic fields that emerge from the G_{SM} symmetry 84 can be described through the Lagrangian in equation 1.2

$$\mathcal{L} = \mathcal{L}_{kin} + \mathcal{L}_\psi + \mathcal{L}_{Yuk} + \mathcal{L}_\phi \quad (1.2)$$

85 Each term in this Lagrangian describes a set of specific particle physics interactions. \mathcal{L}_{kin} 86 . with three families of quarks and leptons, and a scalar Higgs doublet. The standard model 87 has 12 gauge bosons: 8 gluons, 3 weak bosons, and the photon. [1]

88 The physics of the Standard Model of particle physics (SM) is summarized by the SM La- 89 grangian:

$$\mathcal{L}_{kin} = -\frac{1}{4}F_{\mu\nu}F^{\mu\nu} \quad (1.3)$$

90 Explain equation

91 Explain phenomonolyg

92

93

Chapter 2: The Large Hadron Collider

94 The Large Hadron Collider (LHC) is a 26.7km circular high-energy particle accelerator, span-
95 ning the Swiss-French border near the city of Geneva, Switzerland [2]. The LHC occupies the
96 tunnel constructed in 1989 for the Large Electron-Positron (LEP) Collider, and reaches a maxi-
97 mum depth of 170m below the surface. The LHC is operated by the European Organization for
98 Nuclear Research (CERN), the largest international scientific collaboration in the world.

99

100 The LHC accelerates protons and heavy ions and collides them at four interaction points around
101 the ring, with a design center-of-mass energy per collision of $\sqrt{s} = 14$ TeV. Each interaction point
102 is home to one of four detector experiments, which study the products of the collisions. The largest
103 of these experiments is the ATLAS detector, a general purpose detector designed to study the Stan-
104 dard Model and search for new physics that could be produced in LHC collisions [3]. The CMS
105 detector is another general purpose detector, designed and operated independently of the ATLAS
106 detector, but intended to probe the same range of physics [4]. The ALICE experiment is a dedi-
107 cated heavy ion experiment, and the LHC-b experiment is a dedicated *b*-physics experiment [5] [6].

108

109 **2.1 LHC Timeline**

110 The first proton-proton collisions at the LHC were achieved in 2010 with a center-of-mass
111 energy of $\sqrt{s} = 7$ TeV. Run 1 of the LHC took place between 2010 and 2013. The data collected
112 during this time led to the discovery of the Higgs Boston in 2012 [7]. Between 2013 and 2015
113 the LHC underwent the first Long Shutdown (LS1) during which time key upgrades to the physics
114 detectors and the accelerator chain were installed. Run 2 of the LHC took place from 2015 to 2018



Figure 2.1: Timeline of LHC activities [9]

and achieved a center-of-mass energy of $\sqrt{s} = 13$ TeV. Between 2018 and 2022 the LHC underwent its second Long Shutdown (LS2). Run-3 of the LHC began in 2022 and achieved a center-of-mass energy of $\sqrt{s} = 13.6$ TeV. Run-3 is scheduled to continue through 2026, at which point the LHC machine and detectors will undergo upgrades for the *high luminosity* LHC (HL-LHC), which will increase the number of collisions by a factor of 5-10 with respect to the nominal LHC design [8].

2.2 Accelerator Physics

2.2.1 The Journey of a Proton

Protons which feed the LHC start as hydrogen gas. The electrons are removed from the hydrogen atoms through the use of strong electric fields. The linear accelerator (LINAC) then accelerates the H^- ions to an energy of 50 MeV. From here the H^- ions enter the Proton Synchrotron booster, where they are accelerated up to 1.4 GeV of energy. Subsequently they are sorted into bunches separated in time by 25 ns, where each bunch contains approximately 10^{11} protons. Next the bunches pass through the Proton Synchrotron (PS) and the Super Proton Synchrotron (SPS), where they reach energies of 25 GeV and 450 GeV respectively. Finally they are injected into the LHC as two

The CERN accelerator complex Complexe des accélérateurs du CERN

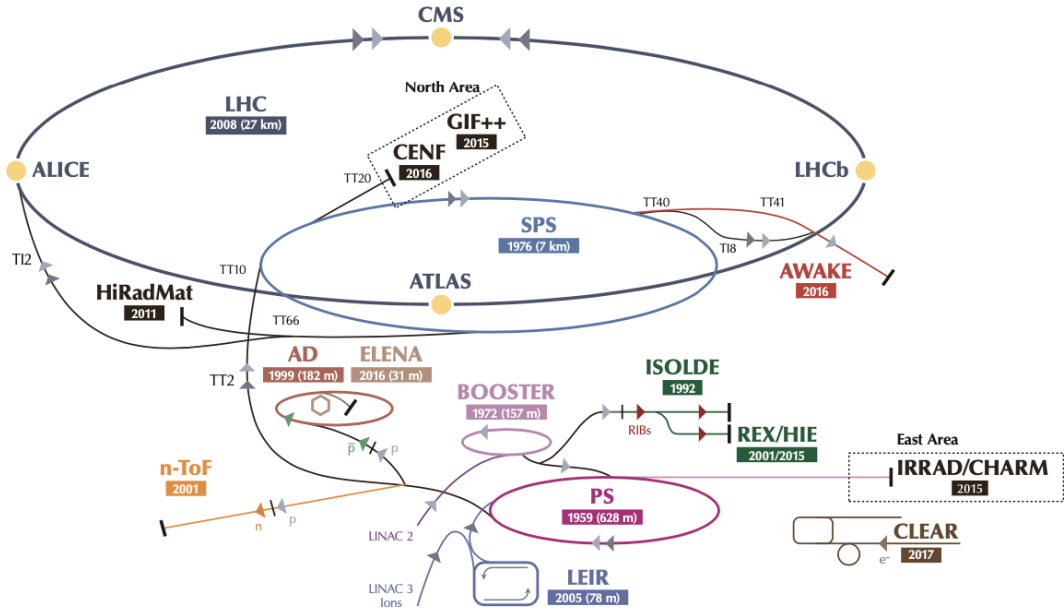


Figure 2.2: The LHC accelerator complex at CERN [11]

beams traveling in opposite direction. The original design allowed each beam to be accelerated up to 7 TeV of energy. Due to limitations with the magnet training, the highest energy actually achieved by the LHC beams during Run 2 was 6.5 TeV, giving a collision center-of-mass energy of $\sqrt{s} = 13$ TeV [10]. Figure 2.2 shows the full LHC accelerator complex.

134

Acceleration in the LHC is performed by eight radio frequency (RF) cavities located around the ring. Each RF cavity produces a 2MV electric field oscillating at 40 MHz. The 40MHz oscillation produces a point of stable equilibrium every 2.5ns. These points of equilibrium are synchronized with the occurrence of the proton bunches produced in the PS – a proton bunch occupies one out of every ten points of stable equilibrium, such that the bunches maintain a 25ns spacing [10].

140

141 2.2.2 Magnets

142 In addition to the acceleration cavities, the LHC houses 9593 superconducting magnets which
143 direct and focus the proton beam on its 27 kilometer journey. The magnets are comprised of super-
144 conducting Niobium-Titanium coils cooled to 1.9K by superfluid helium. As the beams approach
145 one of the four collision points around the ring, multipole magnets focus and squeeze the beam for
146 optimal collisions [10].

147 The LHC is divided into sections, where each section contains an a smoothly curving *arc* and
148 a straight *insertion*. The arcs are composed of 1232 large dipole magnets which bend the beam
149 to follow the roughly circular 27 km path. The main dipoles generate powerful 8.3 tesla magnetic
150 fields to achieve this bend. Each dipole magnet is 15 meters long and weighs 35 tonnes. The
151 dipoles work in conjunction with quadrupole magnets, which keep the particles in a focused beam,
152 and smaller sextupole, octupole and decapole magnets which tune the magnetic field at the ends of
153 the dipole magnets [12].

154 The straight insertion sections have different purposes depending on their location around the
155 ring: beam collisions, beam injection, beam dumping, or beam cleaning. At the four collision
156 points, insertion magnets squeeze the beam to ensure a highly focused collision. This is accom-
157 plished with a triplet of quadrupole magnets, which tighten the beam from 0.2 millimeters to just
158 16 micrometers in diameter. Insertion magnets also clean the beam, which prevents stray particles
159 from hitting sensitive components throughout the LHC. When the LHC is ready to dispose of a
160 beam of particles, beam dump magnets deflect the path of the beam into a straight line towards
161 a block of concrete and graphite that stops the beam. A dilution magnet then reduces the beam
162 intensity by a factor of 100,000 before the final stop [12]. Figure 2.3 shows the locations various
163 beam activities.

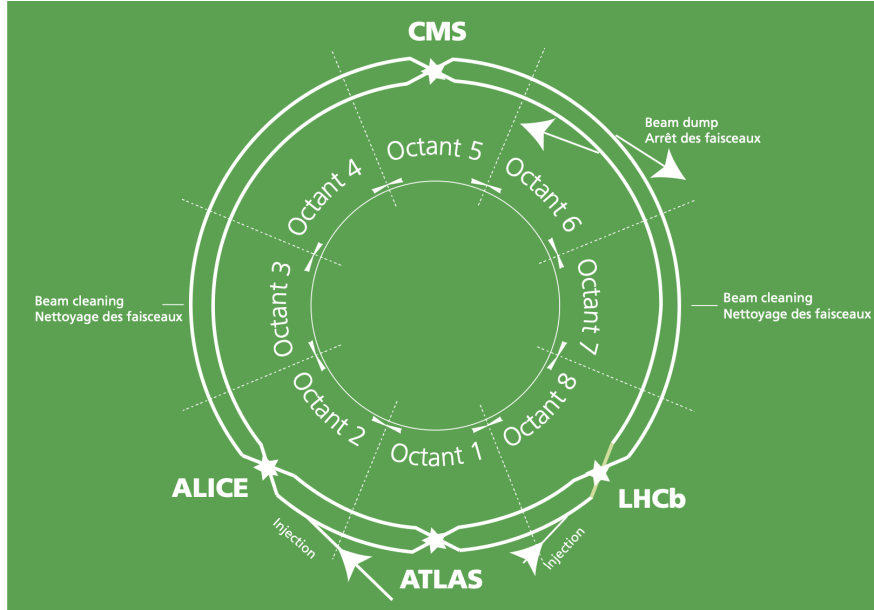


Figure 2.3: The octants of the LHC and location of various beam activities [10]

¹⁶⁴ 2.3 Luminosity

¹⁶⁵ Collisions at the LHC occur when the two beams of proton bunches cross at one of the four
¹⁶⁶ interaction points. The intensity of collisions is described by the instantaneous luminosity, the
¹⁶⁷ formula for which is given in equation 2.1.

$$L = \frac{f N_1 N_2}{4\pi \sigma_x \sigma_y} \quad (2.1)$$

¹⁶⁸ Here f is the revolution frequency, N_1 and N_2 are the number of particle per bunch for each
¹⁶⁹ beam, and σ_x , σ_y are the horizontal and vertical beam widths.

¹⁷⁰

¹⁷¹ The instantaneous luminosity gives the number of the collisions that could be produced at the
¹⁷² interaction point per cm^2 of cross-sectional area per second. The integrated luminosity is obtained
¹⁷³ by integrating the instantaneous luminosity over a given block of time, and measures the total num-
¹⁷⁴ ber of collisions which has occurred during that operation period. This is directly correlated with
¹⁷⁵ the size of the datasets collected by the LHC experiments.

176

177 The design peak luminosity of the LHC is $1.0 \times 10^{34} \text{ cm}^{-2}\text{s}^{-1}$. During Run 1 of the LHC the
178 peak instantaneous luminosity was $0.8 \times 10^{34} \text{ cm}^{-2}\text{s}^{-1}$. Over the course of Run 1 the LHC collected
179 a total integrated luminosity of 5.46 fb^{-1} at $\sqrt{s} = 7 \text{ TeV}$, and 22.8 fb^{-1} at $\sqrt{s} = 8 \text{ TeV}$. Following the
180 first long shutdown and upgrade phase of operations, the LHC achieved a center of mass energy
181 $\sqrt{s} = 13 \text{ TeV}$ at the beginning of Run 2 in 2015. The LHC was also able to deliver 2.0×10^{34}
182 $\text{cm}^{-2}\text{s}^{-1}$ peak instantaneous luminosity, double the design value. During LHC Run 2, from 2015-
183 2018, the LHC delivered 156 fb^{-1} of integrated luminosity for proton-proton collisions. Run 3 of
184 the LHC began in 2022, and is expected to deliver 250 fb^{-1} of integrated luminosity to the ATLAS
185 and CMS experiments by 2026 [9].

186

187 The goal of LHC physic analyses is to find and study rare events produced by interesting
188 physics processes. The cross section σ of a given process indicates the probability of that process
189 occurring given the beam conditions of the LHC. Multiplying the cross section by the integrated
190 luminosity of a dataset gives the expected number of events for that process within the dataset.

$$N_{\text{events}} = \int \sigma L(t) dt = \mathcal{L} \times \sigma \quad (2.2)$$

191 The cross section for most processes of interest, especially BSM processes, is several orders of
192 magnitude below the total cross section for the LHC. Therefore maximizing the number of events
193 produced in collisions is crucial to increase the likelihood of producing events from processes of
194 interest. For this reason, maximizing instantaneous luminosity is a key factor in accelerator design
195 and operation.

196

197

Chapter 3: The ATLAS Detector

198 The ATLAS detector is one of two general purpose physics detectors designed to study the
199 products of the proton-proton collisions produced by the LHC. The detectors is composed of a
200 variety of specialized subsystems, designed to fully capture the large array of physics processes
201 produced in the LHC. The apparatus is 25m high, 44m in length, and weighs over 7000 tons. Colli-
202 sions occur directly in the center of the apparatus, and the cylindrical design of the detector allows
203 a complete 360 view of any physics objects resulting from the collision to be reconstructed.

204

205 Two magnet systems provide strong magnetic fields, which bend the trajectory of charged
206 particles as they pass through the magnetic fields; this allows the calculation of the momentum
207 of the particles. A 2T solenoid magnet provides a uniform magnetic field to the inner layers of
208 the detector. Further out, a toroidal magnet system (TODO: how many toroids?) provides fields
209 strengths of 0.5 to 1T

210 **3.1 Coordinate System and Geometry**

211 The ATLAS detector employs a right hand cylindrical coordinate system. The z axis is aligned
212 with the beam line, and the x-y plane sits perpendicular to the beam line. The origin is centered on
213 the detector, such that the origin corresponds with the interaction point of the two colliding beams.
214 The detector geometry is usually characterized by polar coordinates, where the azimuthal angle ϕ
215 spans the x-y plane. The polar angle θ represents the angle away from the beam line, or z axis.
216 $\theta = 0$ aligns with the positive z -axis, and $\phi = 0$ aligns with the positive x-axis.

217

218 The polar coordinate θ is generally replaced by the Lorentz invariant quantity *rapidity* y .

$$y = \frac{1}{2} \ln\left(\frac{E + p_z}{E - p_z}\right) \quad (3.1)$$

219 This substitution is advantageous because objects in the detector are traveling at highly rela-
 220 tivistic speeds. The relativistic speed of objects passing through the ATLAS detector also means
 221 that the masses of the particles are generally small compared to their total energy. In the limit of
 222 zero mass, the rapidity y reduces to the *pseudorapidity* η , which can be calculated directly from
 223 the polar angle θ .

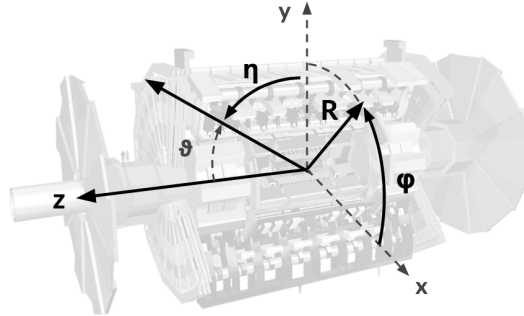
$$\eta = -\ln\left(\frac{\theta}{2}\right) \quad (3.2)$$

224 Figure 3.1a depicts the orientation of the coordinate system with respect to the ATLAS de-
 225 tector, while Figure 3.1b illustrates the relationship between θ , η , and the beamline axis z . The
 226 distance between physics objects in the detector is generally expressed in terms of the solid angle
 227 between them ΔR .

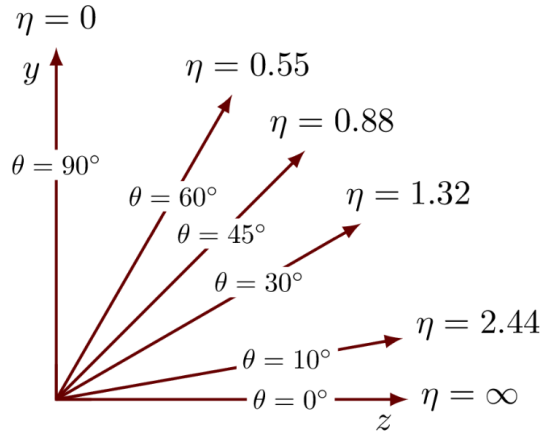
228

$$\Delta R = \sqrt{\Delta\phi^2 + \Delta\eta^2} \quad (3.3)$$

229 Head on proton-proton collisions are more likely to result in objects with a lot of energy in the
 230 transverse plane; glancing proton-proton collisions are more likely to result in objects where most
 231 of the energy is directed along the z -axis. Due to the importance of categorizing these objects,
 232 as well as the cylindrical design of the ATLAS detector, the detector is generally divided
 233 into regions in η . Each subsystem has a “central” or “barrel” region covering low $|\eta|$, while the
 234 “forward” or “endcap” regions cover $|\eta|$ up to 4.9. Each of the three main ATLAS subsystems will
 235 be discussed in the following sections.



(a) The ATLAS geometry



(b) Relationship between η and θ

Figure 3.1: ATLAS coordinate system and geometry

236 3.2 Inner Detector

237 The Inner Detector (ID) is the ATLAS subsystem closest to the interaction point. The primary
 238 purpose of the ID is to determine the charge, momentum, and trajectory of charged particles pass-
 239 ing through the detector. With this information the ID is also able to precisely determine interaction
 240 vertices.

241

242 The ID is composed of three sub-detectors; the pixel detector, the semiconductor tracker (SCT)
 243 and the transition radiation tracker (TRT). Figure 3.2 shows the location of these three subsystems
 244 with respect to each other and the interaction point.

245 3.2.1 Pixel Detector

246 The pixel detector is the first detector encountered by particles produced in LHC collisions.
 247 The original pixel detector consists of 3 barrel layers of silicon pixels, positioned at 4cm, 11cm
 248 and 14cm from the beamline. There are also 4 disks on each side positioned between 11 and 20cm,
 249 providing full coverage $|\eta| < 2.5$. The layers are comprised of silicon pixels each measuring 50
 250 μm by $300 \mu\text{m}$, with 140 million pixels in total. The pixels are organized into modules, which
 251 each contain a set of radiation hard readout electronics chips. In 2014, the Insertable B-layer

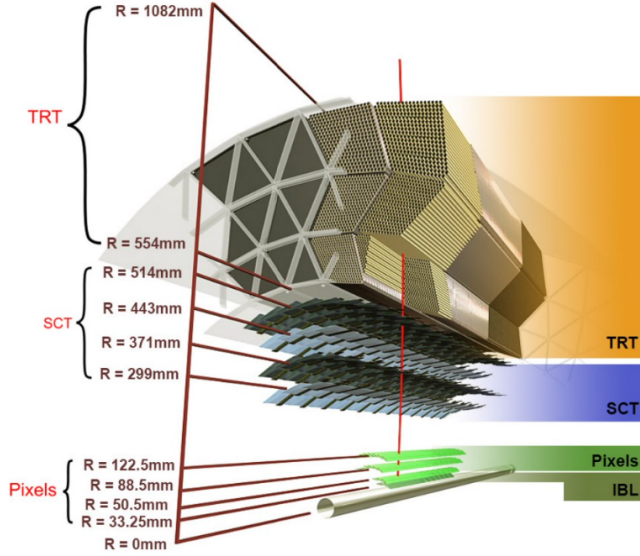


Figure 3.2: A 3D visualization of the structure of the ID in the barrel region [13]

(IBL) was installed, creating a new innermost layer of the pixel detector sitting just 3.3cm from the beamline. The pixels of the IBL measure $50 \mu\text{m}$ by $250 \mu\text{m}$, and cover a pseudo-rapidity range up to $|\eta| < 3$. The IBL upgrade enhances the pixel detector's ability to reconstruct secondary vertices associated with short-lived particles such as the b-quark. The improved vertex identification also helped compensate for increasing pile-up in Run 2.

3.2.2 Semiconductor Tracker

The SCT provides at least 4 additional measurements of each charged particle. It employs the same silicon technology as the Pixel Detector, but utilizes larger silicon strips which measure $80\mu\text{m}$ by 12.4cm. The SCT is composed of 4 barrel layers, located between 30cm and 52cm from the beamline, and 9 end-cap layers on each side. The SCT can distinguish tracks that are separated by at least $200\mu\text{m}$.

3.2.3 Transition Radiation Tracker

The TRT provides an additional 36 hits per particle track. The detector relies on gas filled straw tubes, a technology which is intrinsically radiation hard. The straws which are each 4mm in

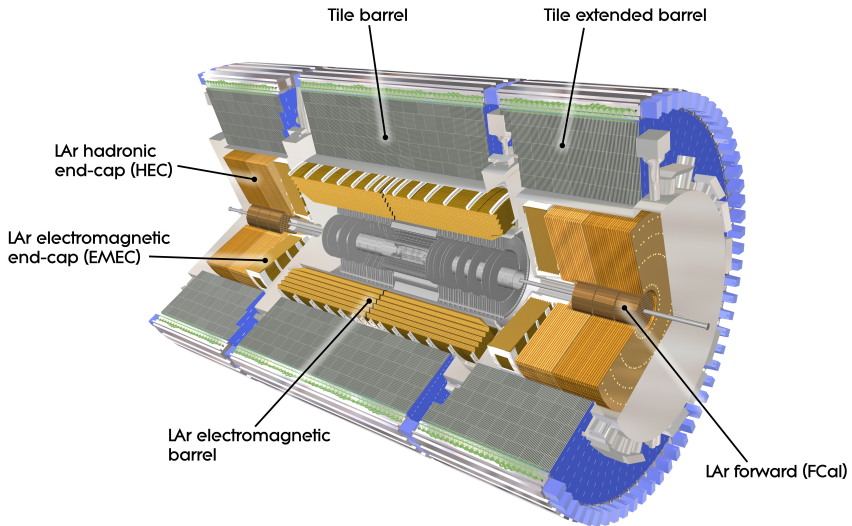


Figure 3.3: ATLAS calorimetry system [14]

266 diameter and up to 150cm in length and filled with xenon gas. The detector is composed of about
 267 50000 barrel region straws and 640000 end-cap straws, comprising 420000 electronic readout
 268 channels. Each channel provides a drift time measurement with a spatial resolution of $170\mu\text{m}$
 269 per straw. As charged particles pass through the detector and interact with the xenon, transition
 270 radiation is emitted. The use of two different drift time thresholds allows the detector to distinguish
 271 between tracking hits and transition radiation hits.

272 3.3 Calorimeters

273 The ATLAS calorimeter system is responsible for measuring the energy of electromagnetically
 274 and hadronically interacting particles passing through the detector. The calorimeters are located
 275 just outside the central solenoid magnet, which encloses the inner detectors. The calorimeters also
 276 stop most known particles, with the exception of muons and neutrinos, preventing them from
 277 traveling to the outermost layers of the detector. The ATLAS calorimetry system is composed of
 278 two subsystems - the Liquid Argon (LAr) calorimeter for electromagnetic calorimetry and the Tile
 279 calorimeter for hadronic calorimetry. The full calorimetry system is shown in figure 3.3.

280 3.3.1 Liquid Argon Calorimeter

281 The LAr calorimeter is a sampling calorimeter designed to trigger on and measure the energies
282 of electromagnetic particles, as well as hadronic particles in the high η regions. It is divided in sev-
283 eral regions, as shown in Figure 3.3. For the region $|\eta| < 1.4$, the electromagnetic barrel (EMB) is
284 responsible for electronic calorimetery, and provides high resolution energy, timing, and position
285 measurements for electrons and photons passing through the detector. The electromagnetic endcap
286 (EMEC) provides additional EM calorimetery up to $|\eta| < 3.2$. In the region $1.4 < |\eta| < 3.2$, the
287 hadronic endcap (HEC) provides hadronic calorimetery. For hadronic calorimetery In the region
288 $|\eta| < 1.4$, corresponding to a detector radii $> 2.2\text{m}$, the less expensive tile calorimeter (discussed
289 in the next section) is used instead. A forward calorimeter (FCAL) extends the hadronic calorime-
290 tery coverage up to $3.1 < |\eta| = 4.8$ [15].

291

292 The LAr calorimeter is composed of liquid argon sandwiched between layers of absorber mate-
293 rial and electrodes. Liquid argon is advantageous as a calorimeter active medium due to its natural
294 abundance and low cost, chemical stability, radiation tolerance, and linear response over a large
295 energy range [16]. The calorimeter is cooled to 87k by three cryostats: one barrel cryostat encom-
296 passing the EMB, and two endcap cryostats. The barrel cryostat also encloses the solenoid which
297 produces the 2T magnetic field for the inner detector. Front end electronics are housed outside the
298 cryostats and are used to process, store and transfer the calorimeter signals.

299

300 **Electromagnetic Calorimeter**

301 For the electromagnetic calorimeters, the layers of electrodes and absorber materials are ar-
302 ranged in an an accordion shape, as illustrated in Figure 3.4. The accordion shape ensures that
303 each half barrel is continuous in the azimuthal angle, which is a key feature for ensuring consistent
304 high resolution measurements. Liquid argon permeates the space between the lead absorber plates,
305 and a multilayer copper-polymide readout board runs through the center of the liquid argon filled

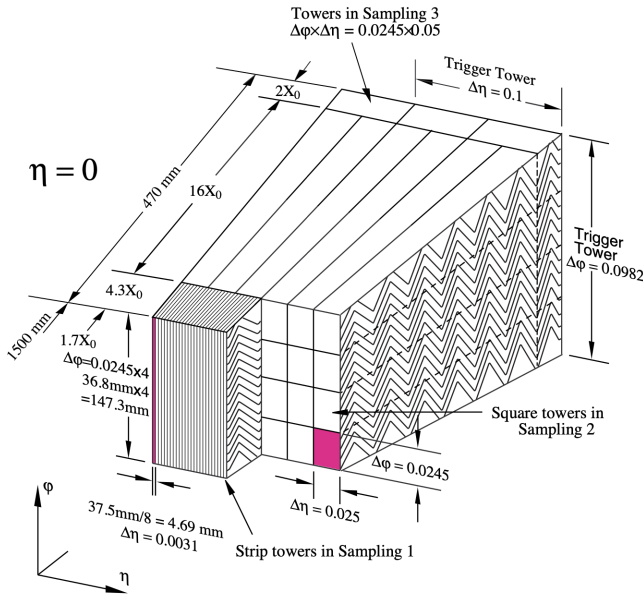


Figure 3.4: Diagram of a segment of the EMB, demonstrating the accordion plate arrangement [15]

306 gap.

307

308 The detection principle for the LAr calorimeter is the current created by electrons which are
 309 released when a charged particle ionizes the liquid argon. In the barrel region, the electrons are
 310 driven towards the center electrodes by a 2000V potential with a drift time of less than 450ns [17].

311 In the endcaps the voltage varies as a function of the radius in order to maintain a flat response [15].

312 The amount of current produced by the ionized electrons is proportional to the energy of the parti-
 313 cle creating the signal. Figure ?? shows the shape of the signal produced in the LAr calorimeter,
 314 before and after it undergoes shaping during the readout process. The shaping of the pulse enforces
 315 a positive peak and a negative tail, which ensures that subsequent pulses can be separated with
 316 the precision required for the 25ns LHC bunch spacing [15].

317

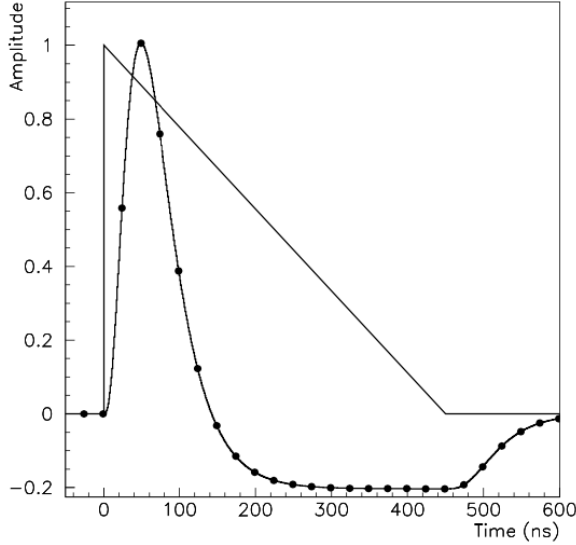


Figure 3.5: A LAr pulse as produced in the detector (triangle) and after shaping (curve) [15]

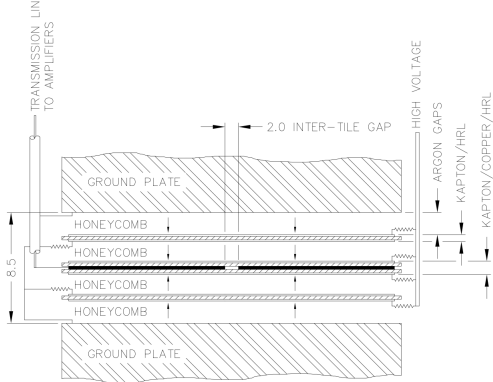


Figure 3.6: Readout gap structure in HEC [15]

318 Hadronic End-cap Calorimeter

319 The HEC sits radially beyond the EMEC. The copper absorber plates in the HEC are oriented
 320 perpendicular to the beamline, with LAr as the active medium. Each end-cap is divided into two
 321 independent wheels; the inner wheel uses 25mm copper plates, while the outer wheel uses 50mm
 322 plates as a cost saving measure. In each wheel, the 8.5mm plate gap is crossed by three parallel
 323 electrodes, creating an effective drift distance of 1.8mm. This gap is illustrated in Figure 3.6.
 324 Each wheel is divided into 32 wedge-shaped modules, each containing their own set of readout
 325 electronics.

326 **Forward Calorimeter**

327 The forward range is covered by the FCAL, which provides both EM and hadronic calorimetry.
328 It is composed of three active cylindrical modules; one EM module with copper absorber plates,
329 and two hadronic modules with tungsten absorber plates. The plates are oriented perpendicular
330 to the beamline, and LAr is used as the active material throughout. The electrodes of the FCal
331 consist of tubes that run parallel to the beam line, arranged in a honeycomb pattern. The resulting
332 LAr gaps are as small as $250 \mu\text{m}$, which enables the FCal to handle the high luminosities and the
333 resulting large influx of particles in the forward region [15].

334 3.3.2 Tile Calorimeter

335 The tile calorimeter (TileCal) provides hadronic calorimetry in the region $\eta < 1.7$, and sur-
336 rounds the LAr calorimeter. It is responsible for measurements of jet energy and jet substructure,
337 and also plays an important role in electron isolation and triggering (including muons) [18]. Tile-
338 Cal is composed of 3 sections, as shown in figure 3.3; a barrel calorimeter sits directly outside the
339 LAr EMB and provides coverage up to $\eta < 1.0$. Two extended barrel sections sit outside the LAr
340 endcaps and cover the region $0.8 < \eta < 1.7$.

341

342 TileCal is a sampling calorimeter composed of steel and plastic scintillator plates as illustrated
343 in Figure 3.7. A total of 460,000 scintillators are read out by wavelength-shifting fibers. The
344 fibers are gathered to define cells and in turn read out by photomultiplier tubes, which amplify
345 the signal and convert it to an electrical signature. Each cell has an approximate granularity of
346 $\Delta\eta \times \Delta\phi = 0.1 \times 0.1$. Each barrel is divided azimuthally into 64 independent modules, an example
347 of which is show in Figure 3.7. The modules are each serviced by front-end electronic housed in a
348 water-cooled drawer on the exterior of the module.

349

350 The detection principle of the TileCal is the production of light from hadronic particles inter-
351 acting with the scintillating tiles. When a hadronic particle hits the steel plate, a shower of particles

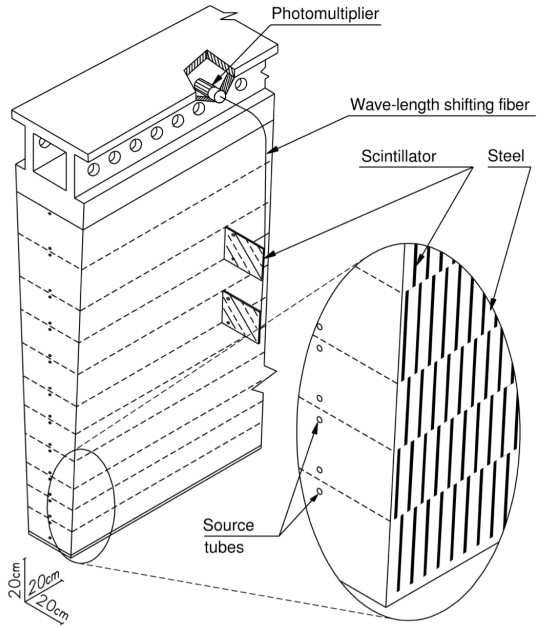


Figure 3.7: TileCal wedge module [18]

352 are produced. The interaction of the shower with the plastic scintillator produces photons, the num-
 353 ber and intensity of which are proportional to the original particle's energy.

354

355 3.4 Muon Spectrometer

356 Unlike electrons, photons, and hadrons, muons interact minimally with the ATLAS calorime-
 357 ters, and can pass through large amounts of detector material without stopping. The ATLAS muon
 358 spectrometer (MS) provides additional tracking information to improve the identification and mea-
 359 surement of muons. The MS comprises the outermost layers of the detector, and is interspersed
 360 with toroid magnets (discussed in section 3.5), which provide a magnetic field of approximately
 361 0.5T. The magnetic field bends the trajectory of the muons as they pass through the detector, and
 362 the degree of the bend is directly correlated with the muon momentum. The path of the muon
 363 is primarily measured by hits in three layers of monitored drift tube (MDT) precision chambers,
 364 which cover the range $|\eta| < 2.7$. The barrel layout of the MS is show in Figure 3.8.

365

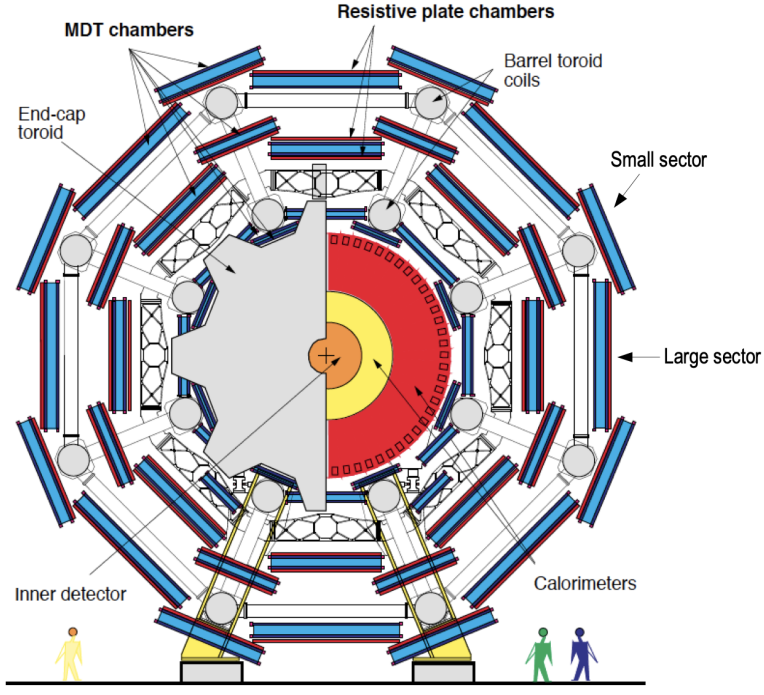


Figure 3.8: Cross section view of the muon spectrometer system [19]

366 Muon triggering is provided by three layers of resistive place chambers (RPC) in the barrel
 367 ($|\eta| < 1.05$), and 3-4 layers of thin gap chambers (TGC) in the endcaps ($1.05 < |\eta| < 2.4$). RPCs
 368 and TGCs also provide muon track measurements in the non-bending coordinate (ϕ). RPCs are
 369 constructed from two parallel resistive plates separated by a 2mm gap filled with a sensitive gas
 370 mixture. This provides a total of six independent measurements for each muon track, with a spatial
 371 resolution of 1cm and a time resolution of 1ns. Time measurements from the RPCs are primarily
 372 associated to hits in the MDT precision chambers to correct the bunch crossing. The time mea-
 373 surement is also used to reject cosmic muons, and to search for delayed signals. TCGs provide
 374 triggering in the endcap regions, and consist of parallel 30 μm wires suspended in a sensitive gas
 375 mixture. TCGs provide high radiation tolerance and a fast response time, both features that are
 376 necessary for handling the high flux of muons in the forward region [19].

377

378 Precision measurements of muon momentum and position are primarily achieved by MDTs.
 379 The MDTs are constructed from 30mm diameter tubes, permeated by a gas mixture of 93% Ar and

380 7% CO₂. The average single-tube spatial resolution is 80 μm . Each chamber consists of six drift
381 tube layers, which together provide a muon track segment resolution of 35 μm . The momentum
382 of the muons can be calculated from the bend in the muon trajectory as they pass through the
383 0.5T magnetic field provided by the toroids. For a $p_T = 1 \text{ TeV}$ track, the average p_T resolution is
384 11%. In the inner most endcap wheels, cathode strip chambers (CSC) are used instead of MDTs,
385 covering the region $2.0 < |\eta| < 2.7$. CSCs are multiwire proportional chambers, with a cathode
386 strip readout. The CSCs have a spatial resolution in the range of 50 μm , and a maximum drift time
387 of about 30 ns, which makes them superior for handling the high flux of particles in the forward
388 region [20].

389 3.5 Magnet System

390 The ATLAS magnet system consists of four sets of superconducting magnets: a barrel solenoid,
391 barrel toroid, and two endcap toroids. The solenoid magnet produces a 2T magnetic field respon-
392 sible for bending the trajectories of charged particles as they pass through the inner detector. The
393 three toroid magnets provide a field of 0.5 - 1 T and curve the path of muons passing through the
394 muon spectrometer.

395

396 The inner solenoid magnet is composed of over 9km of niobium-titanium superconductor
397 wires, which are imbedded into strengthen pure aluminum strips. The solenoid is just 4.5 cm
398 thick, which minimizes interactions between the magnet material and particles passing through the
399 detector. It is housed in the LAr cryostat, as described in section 3.3.1, which further reduces the
400 amount of non-detector material required to support the solenoid. The return yoke of the magnet
401 is provided by the iron absorber of the TileCal [21].

402

403 The central ATLAS toroid magnet, providing the magnetic field for the barrel region of the MS,
404 is the largest toroidal magnet ever constructed at 25m in length. The toroid is composed of eight
405 individual coils, each housed in their own cryostat. The toroidal magnetic field is advantageous

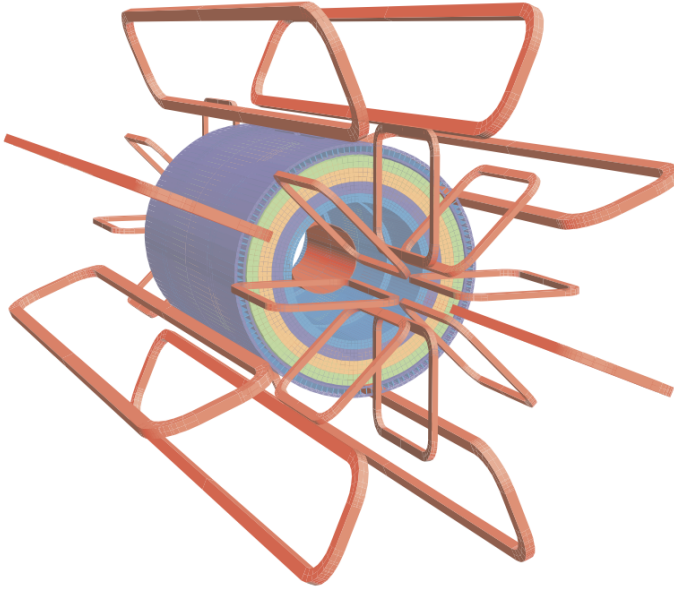


Figure 3.9: Layout of the barrel and endcap toroid magnets [22]

as the direction of the field is almost perpendicular to the path of the charged particles. 56 km of aluminum stabilized niobium-titanium-copper superconductor wire compose the magnet. In each endcap, eight smaller superconducting coils extend the toroidal magnetic field to particles leaving the detector in the forward direction [21]. Figure 3.9 shows the layout of the toroid magnets.

3.6 Forward Detectors

In addition to the inner detector, calorimeters, and muon spectrometer, three smaller detectors provide coverage in the very forward region. The innermost forward detector at 17 m from the interaction point is the LUminosity measurement using Cerenkov Integrating Detector (LUCID). LUCID's primary purpose is to measure the relative online-luminosity for the ATLAS detector, from inelastic $p - p$ scattering. The detector is composed of 20 aluminum Cerenkov tubes which surround the beam pipe and face towards the interaction point. The second forward detector is the Zero-Degree Calorimeter (ZDC), located 140 m from the interaction point in both directions, at the point where the LHC beam-pipe divides into two separate pipes. The ZDC's primary purpose is to detect forward neutrons from heavy ion collisions. The third detector is the Absolute Luminosity

420 for ATLAS (ALFA) system, located 240 m from the interaction point in both directions. ALFA
421 determines luminosity by measuring elastic scattering at small angles, from which luminosity can
422 be calculated via the optical theorem. The detector is built from scintillating fibre trackers, which
423 are connected to the accelerator vacuum via Roman pots, which allow the detector to come as close
424 as 1mm to the beam without disrupting the machine vacuum. The LUCID and ALFA detectors are
425 crucial to determining the real-time conditions of the beams and the total luminosity delivered to
426 the ATLAS detector [22].

427 **3.7 Trigger and Data Acquisition**

428 The trigger and Data Acquisition systems (TDAQ) are responsible for selecting the most viable
429 events to save for further downstream processing. Because of the high luminosities delivered to
430 the ATLAS detector, not all events recorded can be saved; the 40 MHz bunch crossing rate must be
431 reduced by 5 order of magnitude to an event storage rate of 1 kHz. The trigger system is composed
432 of three distinct levels: level 1 (L1), level 2 (L2) and the event filter. Collectively the L2 trigger
433 and the event filter form the high level trigger (HLT).

434

435 The L1 trigger is implemented in the hardware of the ATLAS calorimeter and muon systems.
436 The primary modality of the L1 trigger is to identify muons, electrons, photons, jets, and τ -leptons
437 with high transverse momentum. Particles with high transverse momentum are more likely to
438 originate from direct, high energy collisions, which are most likely to produce interesting physics
439 processes. The L1 trigger also identifies events with large missing transverse energy, which could
440 be indicative of new physics. The L1 muon trigger (L1Muon) relies on RPC and TGC trigger
441 chambers in the barrel and endcap regions of the muon spectrometer. The L1 calorimeter trigger
442 (L1Calo) uses reduced granularity information collected by all the calorimeter subsystems. Results
443 from the L1Muon and L1Calo triggers are combined by the central trigger processor (CTP), which
444 implements a trigger ‘menu’, listing various combinations of trigger requirements. The maximum
445 L1 acceptance rate is 75 kHz, and the L1 trigger decision must reach the front-end electronics

446 within 2.5 μ s of it's associated bunch-crossing [22].

447

448 The L1 trigger defines a Region-of-Interest (RoI) for each passing event. The ROI is repre-
449 sented by the η - ϕ detector region where interesting features were identified by the L1 selection
450 process. Information about the type of feature identified and the threshold exceeded to trigger the
451 L1 response is also recorded. The ROI data is sent to the L2 trigger, which uses all of the available
452 information within the ROI at full granularity and precision. The L2 trigger reduces the event rate
453 from 75 kHz to 3.5 kHz, with an average processing time of 40ms. The final stage of the HLT is
454 the event filter, which reduces the event rate to 200 Hz. The event filter uses an offline analysis
455 process to select fully rebuilt events which will be saved for further analysis.

456

457 All levels of the ATLAS trigger system depend on specialized electronics. Each detector front-
458 end system has a specialized Readout Driver (ROD) which collects data from several front-end
459 data streams at once. The ROD is composed of front-end analogue processing, an L1 buffer which
460 retains the information long enough for the L1 trigger decision, and dedicated links which send the
461 front-end L1 triggered data to data acquisition system (DAQ). Any digital signals are formatted as
462 raw data before being transferred to the DAQ. The first stage of the DAQ temporarily stores the
463 L1 data in local buffers. The ROI data is then requested by the L2 trigger, after which selected
464 events are transferred to an event building system, before events passing the event filter are sent to
465 the CERN computer center for permanent storage. The DAQ system not only allows for the read-
466 out of detector data, but is also responsible for the monitoring and configuration of the hardware
467 and software components which make up the data readout system via the Detector Control System
468 (DCS).

469

470 The DCS allows centralized control of all detector subsystems simultaneously. It continually
471 monitors operational conditions, reports any abnormal behavior to the operator, and can perform
472 both automatic and manual interventions. The DCS reports on real time detector conditions such

⁴⁷³ as high or low voltage detector electronics, gas and cooling systems, magnetic field conditions,
⁴⁷⁴ humidity and temperature. This information is continually monitored by experts in the ATLAS
⁴⁷⁵ control room, so that actions to correct issues can be taken immediately. The DCS also handles
⁴⁷⁶ communication between detector systems, and other systems such as the LHC accelerator, the
⁴⁷⁷ ATLAS magnets, and CERN technical services [22].

Conclusion or Epilogue

479 Use this page for your epilogue or conclusion if applicable; please use only one of the titles
480 for this page. Otherwise, you may delete it. Use this page for your epilogue or conclusion if
481 applicable; please use only one of the titles for this page. Otherwise, you may delete it. Use this
482 page for your epilogue or conclusion if applicable; please use only one of the titles for this page.
483 Otherwise, you may delete it. Use this page for your epilogue or conclusion if applicable; please
484 use only one of the titles for this page. Otherwise, you may delete it. Use this page for your
485 epilogue or conclusion if applicable; please use only one of the titles for this page. Otherwise,
486 you may delete it. Use this page for your epilogue or conclusion if applicable; please use only one
487 of the titles for this page. Otherwise, you may delete it. Use this page for your epilogue or
488 conclusion if applicable; please use only one of the titles for this page. Otherwise, you may delete
489 it. Use this page for your epilogue or conclusion if applicable; please use only one of the titles for
490 this page. Otherwise, you may delete it. Use this page for your epilogue or conclusion if
491 applicable; please use only one of the titles for this page. Otherwise, you may delete it. Use this
492 page for your epilogue or conclusion if applicable; please use only one of the titles for this page.
493 Otherwise, you may delete it. Use this page for your epilogue or conclusion if applicable; please
494 use only one of the titles for this page. Otherwise, you may delete it. Use this page for your
495 epilogue or conclusion if applicable; please use only one of the titles for this page. Otherwise,
496 you may delete it. Use this page for your epilogue or conclusion if applicable; please use only one
497 of the titles for this page. Otherwise, you may delete it. Use this page for your epilogue or
498 conclusion if applicable; please use only one of the titles for this page. Otherwise, you may delete

499 it. Use this page for your epilogue or conclusion if applicable; please use only one of the titles for
500 this page. Otherwise, you may delete it. Use this page for your epilogue or conclusion if
501 applicable; please use only one of the titles for this page. Otherwise, you may delete it. Use this
502 page for your epilogue or conclusion if applicable; please use only one of the titles for this page.
503 Otherwise, you may delete it. Use this page for your epilogue or conclusion if applicable; please
504 use only one of the titles for this page. Otherwise, you may delete it. Use this page for your
505 epilogue or conclusion if applicable; please use only one of the titles for this page. Otherwise,
506 you may delete it. Use this page for your epilogue or conclusion if applicable; please use only one
507 of the titles for this page. Otherwise, you may delete it. Use this page for your epilogue or
508 conclusion if applicable; please use only one of the titles for this page. Otherwise, you may delete
509 it. Use this page for your epilogue or conclusion if applicable; please use only one of the titles for
510 this page. Otherwise, you may delete it. Use this page for your epilogue or conclusion if
511 applicable; please use only one of the titles for this page. Otherwise, you may delete it. Use this
512 page for your epilogue or conclusion if applicable; please use only one of the titles for this page.
513 Otherwise, you may delete it. Use this page for your epilogue or conclusion if applicable; please
514 use only one of the titles for this page. Otherwise, you may delete it. Use this page for your
515 epilogue or conclusion if applicable; please use only one of the titles for this page. Otherwise,
516 you may delete it. Use this page for your epilogue or conclusion if applicable; please use only one
517 of the titles for this page. Otherwise, you may delete it. Use this page for your epilogue or
518 conclusion if applicable; please use only one of the titles for this page. Otherwise, you may delete
519 it. Use this page for your epilogue or conclusion if applicable; please use only one of the titles for
520 this page. Otherwise, you may delete it. Use this page for your epilogue or conclusion if
521 applicable; please use only one of the titles for this page. Otherwise, you may delete it. Use this
522 page for your epilogue or conclusion if applicable; please use only one of the titles for this page.
523 Otherwise, you may delete it. Use this page for your epilogue or conclusion if applicable; please
524 use only one of the titles for this page. Otherwise, you may delete it. Use this page for your
525 epilogue or conclusion if applicable; please use only one of the titles for this page. Otherwise,

526 you may delete it. Use this page for your epilogue or conclusion if applicable; please use only one
527 of the titles for this page. Otherwise, you may delete it. Use this page for your epilogue or
528 conclusion if applicable; please use only one of the titles for this page. Otherwise, you may delete
529 it. Use this page for your epilogue or conclusion if applicable; please use only one of the titles for
530 this page. Otherwise, you may delete it. Use this page for your epilogue or conclusion if
531 applicable; please use only one of the titles for this page. Otherwise, you may delete it. Use this
532 page for your epilogue or conclusion if applicable; please use only one of the titles for this page.
533 Otherwise, you may delete it. Use this page for your epilogue or conclusion if applicable; please
534 use only one of the titles for this page. Otherwise, you may delete it. Use this page for your
535 epilogue or conclusion if applicable; please use only one of the titles for this page. Otherwise,
536 you may delete it. Use this page for your epilogue or conclusion if applicable; please use only one
537 of the titles for this page. Otherwise, you may delete it. Use this page for your epilogue or
538 conclusion if applicable; please use only one of the titles for this page. Otherwise, you may delete
539 it. Use this page for your epilogue or conclusion if applicable; please use only one of the titles for
540 this page. Otherwise, you may delete it. Use this page for your epilogue or conclusion if
541 applicable; please use only one of the titles for this page. Otherwise, you may delete it. Use this
542 page for your epilogue or conclusion if applicable; please use only one of the titles for this page.
543 Otherwise, you may delete it. Use this page for your epilogue or conclusion if applicable; please
544 use only one of the titles for this page. Otherwise, you may delete it. Use this page for your
545 epilogue or conclusion if applicable; please use only one of the titles for this page. Otherwise,
546 you may delete it. Use this page for your epilogue or conclusion if applicable; please use only one
547 of the titles for this page. Otherwise, you may delete it. Use this page for your epilogue or
548 conclusion if applicable; please use only one of the titles for this page. Otherwise, you may delete
549 it. Use this page for your epilogue or conclusion if applicable; please use only one of the titles for
550 this page. Otherwise, you may delete it. Use this page for your epilogue or conclusion if
551 applicable; please use only one of the titles for this page. Otherwise, you may delete it. Use this
552 page for your epilogue or conclusion if applicable; please use only one of the titles for this page.

553 Otherwise, you may delete it. Use this page for your epilogue or conclusion if applicable; please
554 use only one of the titles for this page. Otherwise, you may delete it. Use this page for your
555 epilogue or conclusion if applicable; please use only one of the titles for this page. Otherwise,
556 you may delete it. Use this page for your epilogue or conclusion if applicable; please use only one
557 of the titles for this page. Otherwise, you may delete it. Use this page for your epilogue or
558 conclusion if applicable; please use only one of the titles for this page. Otherwise, you may delete
559 it. Use this page for your epilogue or conclusion if applicable; please use only one of the titles for
560 this page. Otherwise, you may delete it. Use this page for your epilogue or conclusion if
561 applicable; please use only one of the titles for this page. Otherwise, you may delete it. Use this
562 page for your epilogue or conclusion if applicable; please use only one of the titles for this page.
563 Otherwise, you may delete it. Use this page for your epilogue or conclusion if applicable; please
564 use only one of the titles for this page. Otherwise, you may delete it. Use this page for your
565 epilogue or conclusion if applicable; please use only one of the titles for this page. Otherwise,
566 you may delete it. Use this page for your epilogue or conclusion if applicable; please use only one
567 of the titles for this page. Otherwise, you may delete it. Use this page for your epilogue or
568 conclusion if applicable; please use only one of the titles for this page. Otherwise, you may delete
569 it. Use this page for your epilogue or conclusion if applicable; please use only one of the titles for
570 this page. Otherwise, you may delete it. Use this page for your epilogue or conclusion if
571 applicable; please use only one of the titles for this page. Otherwise, you may delete it. Use this
572 page for your epilogue or conclusion if applicable; please use only one of the titles for this page.
573 Otherwise, you may delete it. Use this page for your epilogue or conclusion if applicable; please
574 use only one of the titles for this page. Otherwise, you may delete it. Use this page for your
575 epilogue or conclusion if applicable; please use only one of the titles for this page. Otherwise,
576 you may delete it. Use this page for your epilogue or conclusion if applicable; please use only one
577 of the titles for this page. Otherwise, you may delete it. Use this page for your epilogue or
578 conclusion if applicable; please use only one of the titles for this page. Otherwise, you may delete
579 it.

References

- [1] M. Tanabashi et al. “Review of Particle Physics”. In: *Phys. Rev. D* 98 (3 2018), pp. 847–851.
- [2] Lyndon Evans and Philip Bryant. “LHC Machine”. In: *Journal of Instrumentation* 3.08 (2008), S08001.
- [3] “The ATLAS Experiment at the CERN Large Hadron Collider”. In: *JINST* 3 (2008). Also published by CERN Geneva in 2010, S08003.
- [4] “The CMS experiment at the CERN LHC”. In: *Journal of Instrumentation* 3.08 (2008), S08004.
- [5] “The ALICE experiment at the CERN LHC”. In: *Journal of Instrumentation* 3.08 (2008), S08002.
- [6] “The LHCb Detector at the LHC”. In: *Journal of Instrumentation* 3.08 (2008), S08005.
- [7] Aad G., et al. (ATLAS Collaboration and CMS Collaboration). “Combined Measurement of the Higgs Boson Mass in pp Collisions at $\sqrt(s) = 7$ and 8 TeV with the ATLAS and CMS Experiments”. In: *Phys. Rev. Lett.* 114 (19 2015), p. 191803.
- [8] O. Aberle et al. *High-Luminosity Large Hadron Collider (HL-LHC): Technical design report*. CERN Yellow Reports: Monographs. Geneva: CERN, 2020.
- [9] *The High-Luminosity LHC*. <https://voisins.web.cern.ch/high-luminosity-lhc-hl-lhc>. Accessed: 2024-01-05.
- [10] Ana Lopes and Melissa Loyse Perrey. *FAQ-LHC The guide*. 2022.
- [11] Esma Mobs. “The CERN accelerator complex in 2019. Complexe des accélérateurs du CERN en 2019”. In: (2019). General Photo.
- [12] *Pulling together: Super Conducting electromagnets*. <https://home.cern/science/engineering/pulling-together-superconducting-electromagnets>. Accessed: 2024-01-05.
- [13] G Aad, B Abbott, and ATLAS Collaboration. “Performance of the reconstruction of large impact parameter tracks in the inner detector of ATLAS”. In: *Eur. Phys. J. C Part. Fields* 83.11 (Nov. 2023).
- [14] Joao Pequenao. *Computer Generated image of the ATLAS calorimeter*. 2008.

- 608 [15] *ATLAS liquid-argon calorimeter: Technical Design Report*. Technical design report. AT-
609 LAS. Geneva: CERN, 1996.
- 610 [16] H A Gordon. “Liquid argon calorimetry for the SSC”. In: () .
- 611 [17] Henric Wilkens and (on behalf ofthe ATLAS LArg Collaboration). “The ATLAS Liquid
612 Argon calorimeter: An overview”. In: *Journal of Physics: Conference Series* 160.1 (2009),
613 p. 012043.
- 614 [18] *Technical Design Report for the Phase-II Upgrade of the ATLAS Tile Calorimeter*. Tech.
615 rep. Geneva: CERN, 2017.
- 616 [19] “Technical Design Report for the Phase-II Upgrade of the ATLAS Muon Spectrometer”. In:
617 () .
- 618 [20] L Pontecorvo. “The ATLAS Muon Spectrometer”. In: (2004). revised version number 1
619 submitted on 2003-07-27 16:31:16.
- 620 [21] *ATLAS magnet system: Technical Design Report, 1*. Technical design report. ATLAS. Geneva:
621 CERN, 1997.
- 622 [22] The ATLAS Collaboration. “The ATLAS Experiment at the CERN Large Hadron Collider”.
623 In: *Journal of Instrumentation* 3.08 (2008), S08003.

Appendix A: Experimental Equipment

626 Lorem ipsum dolor sit amet, consectetur adipiscing elit, sed do eiusmod tempor incididunt ut
627 labore et dolore magna aliqua. Ut enim ad minim veniam, quis nostrud exercitation ullamco laboris
628 nisi ut aliquip ex ea commodo consequat. Duis aute irure dolor in reprehenderit in voluptate velit
629 esse cillum dolore eu fugiat nulla pariatur. Excepteur sint occaecat cupidatat non proident, sunt in
630 culpa qui officia deserunt mollit anim id est laborum.

631

632

Appendix B: Data Processing

633 Lorem ipsum dolor sit amet, consectetur adipiscing elit, sed do eiusmod tempor incididunt ut
634 labore et dolore magna aliqua. Ut enim ad minim veniam, quis nostrud exercitation ullamco laboris
635 nisi ut aliquip ex ea commodo consequat. Duis aute irure dolor in reprehenderit in voluptate velit
636 esse cillum dolore eu fugiat nulla pariatur. Excepteur sint occaecat cupidatat non proident, sunt in
637 culpa qui officia deserunt mollit anim id est laborum.